INTERNATIONAL JOURNAL FOR NUMERICAL METHODS IN FLUIDS, VOL. 24, 813–831 (1997)

MULTIPLE STATES OF A VISCOUS FREE SURFACE FLOW: TRANSITION FROM PRE-METERED TO A METERING INFLOW

M. S. CARVALHO[1] AND L. E. SCRIVEN[1]*

[1]*Coating Process Fundamentals Program, Center for Interfacial Engineering and Department of Chemical Engineering and Material Science, University of Minnesota, Minneapolis, MN 55455, U.S.A.*

SUMMARY

In a forward-roll coating gap or nip, steady laminar flow of liquid between counter-rotating cylinders or rolls is used to split the flow into a coated layer on one roll and a rejected layer on the other. Both layers have free surfaces in contact with air. Liquid may be carried into the gap as a layer on one or both rolls. If the arriving layer is not too thick, all of the liquid flows through the gap, a situation called *pre-metered*. If the arriving layer is too thick, part of the liquid is rejected and runs back down the lower roll. The flow rate through the gap is said to be *metered* and is not known *a priori*.

The transition from a *pre-metered* regime to the *metered* situation was examined by solving the Navier–Stokes system for steady, two-dimensional flow in a domain bounded by free surfaces, two rigid roll surfaces and chosen inflow and outflow surfaces. The *free boundary condition*, as described by Papanastasiou *et al.* (*Int. j. numer methods fluids*, **14**, 587 (1992)), was explored and proved to accommodate both the pre-metered and metered regimes. A run-back flow state across the synthetic inlet plane was obtained, provided a condition on the thickness of the arriving layer was replaced by a kinematic condition at a certain stage.

The coupled equation system was solved by Galerkin's method with finite element basis functions. The resulting non-linear algebraic system was solved by Newton's method with initialization by pseduo-arc-length continuation and automatic parameter step adjustment.

Results show the existence of multiple solutions which can lead to hysteresis. Flow regime maps were constructed to portray the operating parameter range in which a coating bead can exist and the ranges in which a coating gap operates in either the pre-metered or the metering regime. © 1997 by John Wiley & Sons, Ltd. Int. j. numer. methods fluids 24: 813–831, 1997.

(No. of Figures: 18. No. of Tables: 0. No. of Refs: 26.)

KEY WORDS: pre-metered; metered; free boundary condition; free surface flow; viscous

1. INTRODUCTION

In forward-roll coating, liquid is usually carried into the gap between the rolls as a layer or film on one or both of them. Figure 1 illustrates the single-film-fed forward-roll coating flow in which the liquid arrives on the bottom roll. The incoming layer is the outflow of some other unit flow located upstream. It could be formed by a roll dipping liquid out of a pool, by a film split as in the case of a multiple roll coater or by extrusion from a die slit. If the incoming layer thickness is less than the gap

*Correspondence to: L. E. Scriven, Coating Process Fundamentals Program, Center for Interfacial Engineering and Department of Chemical Engineering and Material Science, University of Minnesota, Minneapolis, MN 55455, U.S.A.

CCC 0271–2091/97/090813–19$17.50

Received 11 June 1996

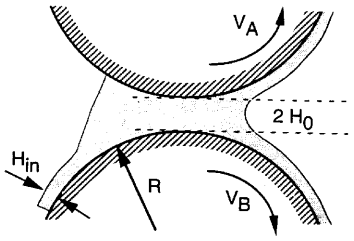

Figure 1. Sketch of single-film-fed forward-roll coating flow

clearance but larger than the minimum value required for a steady flow to exist, the flow rate that goes through the gap is completely determined by the incoming layer, as in the case of meniscus coating (treated by Savage *et al.*[1]). This situation is usually called *pre-metered*. However, if the incoming layer or film is too thick, part of the liquid is rejected and runs back down the lower roll as the outer part of a film flow within which the velocity reverses. At intermediate thicknesses the arriving flow is influenced by what is happening both upstream and downstream. In the last two situations the flow rate through the gap is said to be *metered* and is not known *a priori*. Figure 2 contrasts the different flow states.

Previous analyses of flows in a roll coating gap did not address the inlet condition, i.e. they did not distinguish whether the gap was a metering gap or the flow was premetered. Coyle *et al.*[2] considered only cases in which the rolls are half-submerged, i.e. completely flooded upstream. This condition,

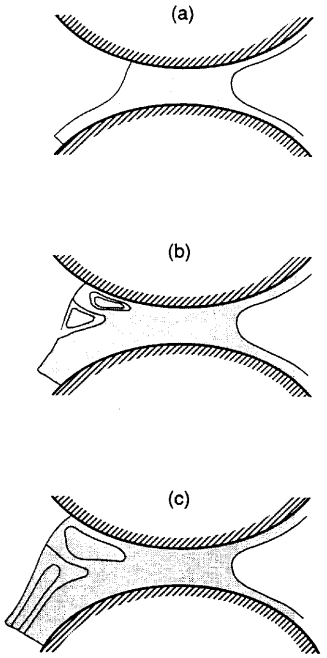

Figure 2. Feed condition in single-film-fed forward-roll coating depends on thickness of arriving liquid layer: (a) starved—pre-metered; (b) flooded (upstream gyre)—influence transmitted upstream; (c) run-back—metered

which is approached in pond-fed gaps, is a convenient boundary condition for estimating the flow rate through forward-roll coating gaps. It models accurately a metering gap in which there is a rolling bank located upstream, as shown in Figures 2(b) and 2(c). Experimental works have replicated the half-flooded condition[3,4] and so it was used to validate theoretical results.

The single-film-fed roll coating flow was first analysed by Chen and Higgins[5] and Chen and Scriven.[6] They considered a pre-metered flow, i.e. the flow rate was set by the incoming liquid layer. At higher flow rates, gyres were found to develop in the flow upstream of the minimum clearance. This rolling bank was visualized by Bourgeois and Agassant[7] and Agassant and Epsy[8] in the flow of molten polymer (very high viscosity) between a pair of rotating rolls at some operating conditions. Benjamin[9] constructed flow regime maps, i.e. quality windows, based on the number of gyres in the flow and their connectivity and analysed their stability with respect to two-dimensional disturbances. He too set the flow rate by fixing the velocity profile at the inflow boundary upstream on the incoming liquid layer. However, some of the cases he treated are at parameter values at which the flow is clearly not pre-metered and the interaction of the imposed inflow boundary condition with the requirements of mass and momentum conservation in the coating bead produced unrealistic shapes of the upstream free surface (Reference 9, pp. 4.26 and 4.31). Savage *et al.*[1] analysed the different patterns of streamlines and gyres, or flow topologies, that can occur in what is called meniscus coating, i.e. at very small capillary numbers and large gaps. The range of parameter values that corresponds to meniscus coating was also covered by Benjamin's[9] flow regime maps. In meniscus coating the flow is always pre-metered (the inlet film is much thinner than the clearance between the rolls) and therefore imposing a velocity profile at the inflow boundary is a satisfactory boundary condition because it does not affect the flow in the coating bead appreciably.

The transition from a pre-metered gap to a metering gap is studied in this work by solving the Navier–Stokes system with the Galerkin/finite element method. In order to analyse the transition, an appropriate boundary condition is needed at the synthetic inflow boundary located upstream where the incoming liquid layer arrives. Because there is not enough information about the arriving flow to impose an accurate condition on the velocity, the use of the so-called *free boundary condition*, as described by Papanastasiou *et al.*,[10] was explored. This boundary condition takes advantage of the option inherent in the Galerkin/finite element method of imposing *no boundary condition* and instead requiring that the momentum equation be satisfied in the weak sense, i.e. that its weighted residual vanish, over the subdomain adjacent and interior to the inflow boundary. Although this procedure is questioned in the light of conventional understanding of partial differential equation theory,[11] it has been used before an *outflow boundary condition* with great success in certain situations.[10,11] In the present case the results show that the free boundary condition yields realistic flow states that extend to both of the extreme situations of interest, namely pre-metered flow and metering gaps. In the latter case it yields run-back velocity profiles, i.e. exiting as well as entering flow, in the synthetic inlet plane, provided a switch is made at a certain stage between specifying the thickness of the pre-metered layer and specifying a kinematic condition at the free surface adjacent to the inflow boundary.

2. GOVERNING EQUATIONS AND METHOD OF SOLUTION

2.1. Governing equations and boundary conditions

The Navier–Stokes system for viscous free surface flows is described in detail by Kistler and Scriven.[12] This section recapitulates the governing equations and lays out the boundary conditions used to study the feed condition.

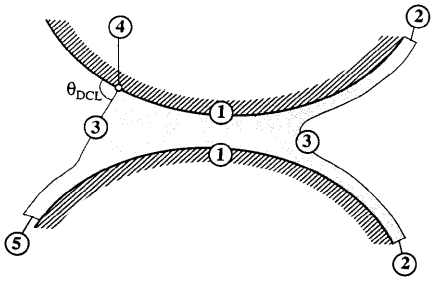

Figure 3. Sketch of flow domain in single-film-fed forward-roll coating flow. θ_{DCL} is the apparent dynamic contact angle

Figure 3 shows the domain used. The velocity and pressure fields are governed by the momentum and continuity equations, which in dimensionless form are

$$Re\ \mathbf{v}\cdot\nabla\mathbf{v}-\nabla\cdot\boldsymbol{\sigma}-St\mathbf{F}=0, \qquad \nabla\cdot\mathbf{v}=0. \tag{1}$$

$\boldsymbol{\sigma}$ is the total stress tensor, the sum of pressure and viscous stress; for a Newtonian liquid it is

$$\boldsymbol{\sigma}=-p\mathbf{I}+\nabla\mathbf{v}+(\nabla\mathbf{v})^{\mathrm{T}}.$$

Velocities are measured in units of average roll speed $\bar{V}\equiv(V_{\mathrm{A}}+V_{\mathrm{B}})/2$. Lengths are written in units of half-gap H_0, i.e. the minimum clearance between the rolls is $2H_0$. $\mathbf{g}$ is a unit vector in the direction of gravity. The Reynolds number $Re\equiv\rho\bar{V}H_0/\mu$ measures the ratio between inertia and viscous forces and the Stokes number $St\equiv\rho gH_0^2/\mu\bar{V}$ the ratio between gravity and viscous forces.

At the rigid roll surfaces (**1**) the no-slip and no-penetration condition applies, i.e.

$$\mathbf{v}=\mathbf{V}_{\mathrm{roll}}. \tag{2}$$

At the chosen outflow boundaries (**2**), which can be regarded as synthetic boundaries, the directional derivative of the velocity is set to zero, a Neumann-type boundary condition:

$$\frac{\partial\mathbf{v}}{\partial\mathbf{n}}\equiv\mathbf{n}\cdot\nabla\mathbf{v}=0. \tag{3}$$

This was chosen over specifying the velocity profile itself, i.e. a Dirichlet condition, because the latter is highly restrictive, generally causing 'wiggles' to appear in the solution.

At the free surfaces (**3**) the traction in the liquid balances the capillary pressure and there is no mass flow across the surface:

$$\mathbf{n}\cdot\boldsymbol{\sigma}=\frac{1}{Ca}\frac{\mathrm{d}\mathbf{t}}{\mathrm{d}s}-\mathbf{n}P_{\mathrm{amb}}, \qquad \mathbf{n}\cdot\mathbf{v}=0. \tag{4}$$

At the dynamic contact line (**4**) the Navier slip condition was used instead of the no-slip condition and a dynamic contact angle $\theta_{\mathrm{DCA}}=130^{\circ}$ was imposed:

$$\frac{1}{\beta}\mathbf{t}_{\mathrm{w}}\cdot(\mathbf{v}-\mathbf{V}_{\mathrm{wall}})=\mathbf{t}_{\mathrm{w}}\cdot(\mathbf{n}_{\mathrm{w}}\cdot\boldsymbol{\sigma}), \qquad \mathbf{n}_{\mathrm{w}}\cdot\mathbf{n}_{\mathrm{fs}}=\cos\theta_{\mathrm{DCA}}. \tag{5}$$

At the chosen inflow boundary (**5**), which can also be regarded as a synthetic boundary, the flow is not known *a priori*, although in the pre-metered case it approaches solid body rotation as the layer is made thinner and thinner and it could be adequately approximated by a Neumann or even a Dirichlet boundary condition. Otherwise there is not enough upstream information and so the *free boundary condition*, advocated by Papanastasiou *et al.*[10] as an outflow boundary condition for flow problems, was tried. The way in which this was done is described in the next subsection.

At the corner between the inflow boundary and the upstream free surface (**6**), two different conditions were explored. The first one consisted of fixing the thickness of the arriving layer, H_{in}, i.e. the co-ordinates of the finite element node located at that corner were fixed. Although the layer thickness was fixed, the flow rate through the gap was not, because the velocity profile at the synthetic inlet boundary was not imposed. The second condition, used to obtain another sequence of computed predictions, was the kinematic condition at the free surface adjacent to the inlet boundary. The switch between the two conditions was made at a set of parameters at which they yielded *almost* identical flow states, and checking by extending each sequence into the province of the other. The switch was necessary because as the upstream recirculation grows and crosses the synthetic inflow plane, the thickness at that plane changes and exiting liquid runs down that which is arriving on the lower roll (Figure 2(c)).

2.2. Solution method

The flow domain is unknown *a priori*. In order to solve the free boundary problem by means of standard techniques for boundary value problems, the set of differential equations posed in the unknown domain has to be transformed to an equivalent set defined in a known reference domain. This transformation is made by a mapping $\mathbf{x} = \mathbf{x}(\boldsymbol{\xi})$ that connects the two domains. Here the unknown physical domain is parametrized by the position vector $\mathbf{x}$ and the reference domain by $\boldsymbol{\xi}$. The choice of reference domain adopted is a matter of convenience. A common approach is to use a simple quadrangular domain tessellated into unit squares. In many situations, however, the physical domain cannot be mapped into a simple quadrangular reference domain. In these situations the physical domain can be subdivided into subdomains (also called regions), each of which can be mapped to quadrangular reference regions. The mapping is arbitrary, except that (i) boundaries of the reference domain have to be continuously mapped onto the boundaries of the physical domain and (ii) the mapping has to be invertible. Finding a mapping that satisfies both conditions is not always an easy task. Theoretical research on mesh generation addresses the issues of existence and uniqueness of such mappings.[13–15] The mapping used here is the one chosen earlier by de Santos[16] and discussed in more detail by Benjamin.[9] They have shown that a functional of weighted smoothness can be used successfully to construct meshes for viscous free surface flows of the kind involved here. The inverse of the mapping that minimizes the functional is governed by a pair of elliptic differential equations identical with those encountered in the dilute regime of diffusional transport with variable diffusion coefficients. The co-ordinate potentials ξ and η satisfy

$$\nabla \cdot (D_\xi \nabla \xi) = 0, \qquad \nabla \cdot (D_\eta \nabla \eta) = 0. \tag{6}$$

D_ξ and D_n are their respective diffusion coefficients. They control the spacing of the curves of constant ξ and η chosen to tessellate the region into finite elements.

The Navier–Stokes system and the mesh generation equations were solved by the Galerkin/finite element method. Biquadratic basis functions were used to represent both the velocity and the mapping from the reference to the physical domain. The basis functions used to represent the pressure field were piecewise, linear and discontinuous.

Boundary conditions are needed in order to solve the second-order partial differential equations (6). Along solid walls and synthetic inlet and outlet planes the boundary is located by imposing a relation between the co-ordinates x and y from the equation that describes the shape of the boundary. The finite element nodes are distributed along a boundary by means of a prescribed distribution function.

Along free surfaces the free boundary is located by imposing the kinematic condition. The corresponding weighted residual is

$$R_i^{\mathrm{k}} = \int_{\Gamma_{\mathrm{fs}}} (\mathbf{n} \cdot \mathbf{v}) \Phi_i \mathrm{d}\Gamma_{\mathrm{fs}}.$$

Previous works on free surface flows (see e.g. References 2, 9, 12 and 17) used the biquadratic basis functions ϕ_i as weighting functions for the kinematic residual, i.e. $\Phi_i = \phi_i$. This approach does not force the total flow rate across the free surface to vanish. Some tests carried out in the course of the present work revealed that the average leakage through the free surfaces was of the order of 10^{-5}–10^{-6} in units of the product of the characteristic velocity V and characteristic length L. This value is quite small compared with the total flow rate in many coating flows. However, if the total flow rate is of the order of $10^{-3}VL$, the leakage can be as high as 5% of the total flow rate. This shortcoming was overcome by changing the weighting functions of the kinematic residual. In order to enforce a vanishing flow rate across free surfaces, one of the weighting functions Φ_i of each element on a free surface was set equal to unity, so that the corresponding weighted residual became

$$R_i^{\mathrm{x}} = \int_{\Gamma_{\mathrm{fs}}} (\mathbf{n} \cdot \mathbf{v}) \mathrm{d}\Gamma_{\mathrm{fs}} = 0.$$

In this way the integral of the flow across the free surface over each element was reduced to the level of truncation error by the computer.

To solve for one sequence of flow states, the three kinematic residuals associated with the corner element between the free surface and the inlet boundary were set to zero. For the other sequence, one was replaced as described in the third paragraph below.

The boundary integrals in the weighted residuals of the x- and y-components of the momentum equation that come from the divergence theorem are

$$(BI)x = -\int_{\Gamma_{\mathrm{e}}} \phi^i [(\mathbf{n} \cdot \boldsymbol{\sigma}) \cdot \mathbf{e}_{\mathrm{x}}] \mathrm{d}S, \qquad (BI)_Y = 0 \int_{\Gamma_{\mathrm{e}}} \phi^i [(\mathbf{n} \cdot \boldsymbol{\sigma}) \cdot \mathbf{e}_{\mathrm{y}}] \mathrm{d}S,$$

where ϕ^i is any of the basis functions with which the momentum equation residual is weighted.

Usually a Neumann or a Robin boundary condition is applied by replacing the liquid traction $\mathbf{n} \cdot \boldsymbol{\sigma}$ that appears in the boundary integral shown above by the external contribution that appears with it in the boundary condition, i.e. by the external traction that balances it. For example, in the case of a liquid/gas interface the liquid traction $\mathbf{n} \cdot \boldsymbol{\sigma}$ is balanced by the capillary pressure jump as represented by equation (4). At the synthetic outlet boundaries (**2**) the directional derivative of velocity is assumed to vanish. The liquid traction is

$$\mathbf{n} \cdot \boldsymbol{\sigma}|_{\Gamma_o} = -p|_{\Gamma_{\mathrm{e}}} \mathbf{n} + \mathbf{n} \cdot (\nabla \mathbf{v})^{\mathrm{T}}|_{\Gamma_{\mathrm{e}}}.$$

At the synthetic inlet boundary (**5**) the traction exerted by the liquid immediately upstream is not known. Thus the liquid traction was simply evaluated immediately downstream of the inflow boundary Γ_{e} from its representation in the finite element basis function set:

$$\mathbf{n} \cdot \boldsymbol{\sigma}|_{\Gamma_{\mathrm{e}}} = -p|_{\Gamma_{\mathrm{e}}} \mathbf{n} + \mathbf{n} \cdot [\nabla \mathbf{v}|_{\Gamma_{\mathrm{e}}} + (\nabla \mathbf{v})^T|_{\Gamma_{\mathrm{e}}}].$$

This condition takes advantage of the option inherent in Galerkin's method of imposing no boundary condition and instead requiring that the momentum equation be satisfied in the weak sense throughout the subdomain adjacent and interior to the inflow boundary.

To solve for the sequence of flow states in which the incoming layer thickness was fixed, the vanishing of the kinematic residual associated with the corner between the free surface and the inflow boundary was replaced by the prescription of the layer thickness there. This alternative can be viewed as imposing a so-called essential boundary condition on the free surface itself.

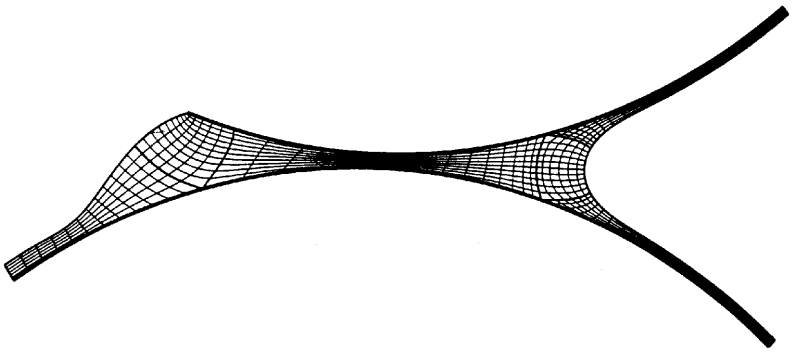

Figure 4. Representative mesh used to discretize problem: 500 elements and 10,112 unknowns

Both of the resulting non-linear systems of algebraic equations for the coefficients of the basis functions were solved by Newton's method with pseudo-arc-length continuation, as described by Keller.[18] The domain was divided into 500 elements with 10,112 unknowns. A representative mesh is shown in Figure 4. Further refinement, e.g. by doubling the number of unknowns and of equations, changed the flow rate and dynamic contact line position only in the fourth significant figure and did not alter the solution path in the space of the operating parameter. Manual remeshing was not used during the continuation process.

The initial guess used to obtain the first solution from which the arc-length continuation began consisted of the velocity and pressure fields obtained by fixing the position of the free surfaces and imposing zero shear stress at those locations.

The computations were made with a Cray X-MP computer and each Newton step took approximately 16 s of CPU time.

3. RESULTS

The influence of the feed condition on the gap performance can be characterized in many ways. At given roll speed, liquid properties and incoming film thickness H_{in} it is desirable to know (i) the range of gaps in which a coating bead can exist, (ii) the sensitivity of the flow rate to the gap, (iii) when the transition from the pre-metered regime to the metered regime occurs and (iv) when there are multiple steady states. Among other possibilities, multiple steady states could be accompanied by limit cycles, i.e. periodically varying flow in the coating bead and periodically varying coated thickness.

The range of parameters explored corresponds to at least some of the practical operating conditions in forward-roll coating:

(a) Reynolds number $Re \equiv \rho \bar{V} H_0/\mu \approx 0$–$1$
(b) Stokes number $St \equiv \rho g H_0^2/\mu \bar{V} \approx 0$–$1$
(c) capillary number $Ca \equiv \mu \bar{V}/\sigma \approx 0{\cdot}1$–$10$
(d) gap/roll radius ratio $H_0/R \approx 10^{-4}$–10^{-2}.

In previous analyses of single-film-fed forward-roll coating flows the effect of gravity has usually been neglected, i.e. $St = 0$.[6,9] In order to compare the predictions of this work with those reported by Benjamin,[9] gravity is neglected in the cases covered in Section 3.1. In Section 3.2 the effect of gravity is studied in the cases where the Stokes number ranges through realistic values.

3.1. Flow states with negligible gravity effects (St = 0)

A simple way to characterize different flow states is by the position of the dynamic contact line where the liquid meets the metering roll. Figure 5 shows how this quantity varies with the clearance between the rolls. The path of flow states, i.e. solutions of the governing equations, was computed at $Ca = 0{\cdot}1$, inlet film thickness $H_{in}/R = 2{\cdot}7 \times 10^{-2}$ and modified Reynolds Number $Re^* \equiv Re \times R/H_0 = 100$. Figure 6 shows the streamlines at particular parameters highlighted in Figure 5.

The stability of the flow was not investigated, i.e. the eigenvalue problem was not solved. Nevertheless, it is well established that the stability of solutions along a branch in parameter space changes at a regular turning point.[19] The topmost branch in Figure 5 (branch A) is highly likely to be unstable. In extreme cases the upstream free surface touches the top roll, air is trapped between the roll surface and the coating liquid, and the coated film that is delivered is defective, as illustrated in Figure 6(a). The stable states are located between turning points #1 and #2 (branch B) and between turning points #3 and #4 (branch D). In Figure 5 these states are represented by full circles and squares respectively.

Turning point #1 sets a maximum distance between the rolls beyond which there is no two-dimensional, steady state solution. In practice this would signal that the coating bead would break up if the rolls were moved apart from flow state (b) (Figure 5).

Tracking the solution path along branch B, from turning point #1 in the direction of narrowing gaps, i.e. bringing the rolls together, shows that the upstream free surface moves away from the plane of the minimum gap. The stable states on most of branch B have no recirculation on the inlet side of the gap (see cases (b) and (c) in Figure 6). Near turning point #2 a small gyre appears on the inlet side of the gap. The flow states of the bottommost branch D, which are highly likely to be stable solutions, are characterized by the presence of a recirculation zone attached to the free surface. As the rolls are pushed together, the gyre moves upstream towards the inlet plane (Cases (d) and (e) in Figure 6). Turning point #4 occurs when the recirculation zone reaches the synthetic inlet boundary. The solution branch beyond this turning point is not shown. Along it the free surface becomes more and more distorted: a bump in the free surface attached to the inlet plane grows, evidently in order to reconcile flow recirculating from closer to the gap with the imposed thickness of the incoming film. This solution is clearly unrealistic and therefore beyond turning point #4 the inlet film thickness cannot be fixed. At this stage the condition of fixed inlet thickness should be replaced by the weighted

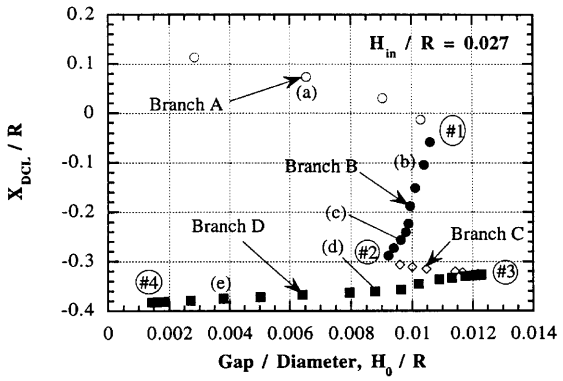

Figure 5. Path of flow states (solutions of governing equations) at $St = 0$, $Ca = 0{\cdot}1$, $H_{in}/R = 0{\cdot}027$ and $Re \times R/H_0 = 100$. The states are characterizied by the position of the dynamic contact line where the liquid meets the metering roll. Streamlines of flow states (a)–(e) are shown in Figure 6

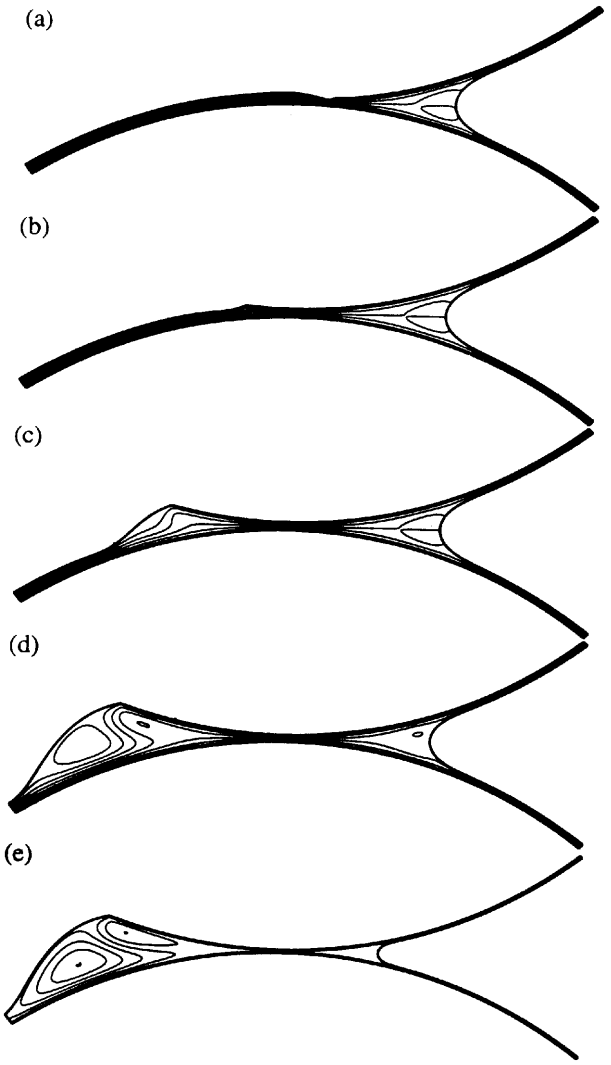

Figure 6. Streamlines of flow states labelled in Figure 5. The inlet film thickness is fixed

kinematic residual at the corner, as described above. However, the corresponding sequence of solutions was explored only with more realistic Stokes numbers (Section 3.2). Moreover, additional solutions with other choices of location of the synthetic inlet boundary showed clearly that the set of parameters at which turning point #4 occurs depends on that location, as expected.

Figure 7 shows how the dimensionless flow rate $q = Q/2\bar{V}R$ varies with the dimensionless gap between the rolls, H_0/R, at the same flow states as in Figure 5. Along segment A (unstable) and most of segment B (stable) the flow rate does not vary perceptibly and its value is close to the product of the arriving film thickness and roll speed, i.e. $Q \approx VH_{\text{in}}$. The small difference arises from the velocity profile in the incoming film not being a plug flow distribution. This is the pre-metered regime: the upstream influence of the gap is negligible at the synthetic inflow boundary; the velocity distribution in the film there is virtually fully developed; and the *free boundary condition* admits this

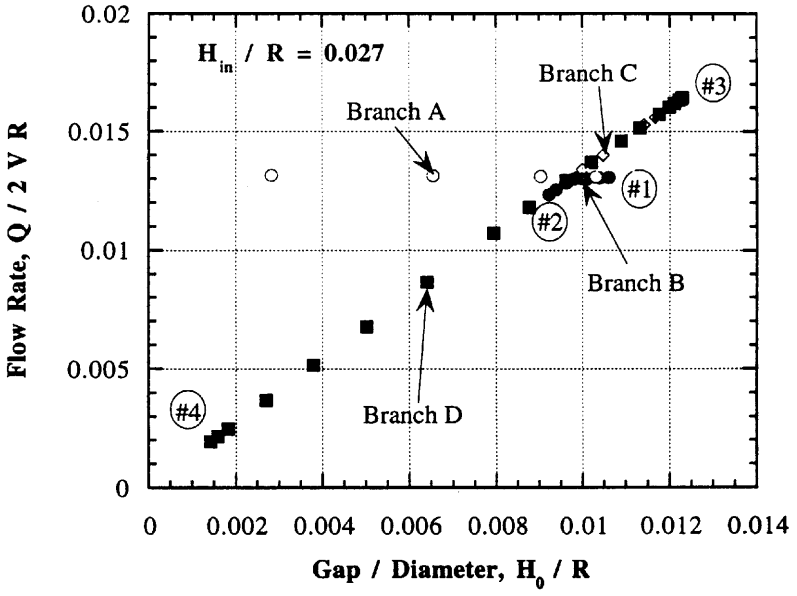

Figure 7. Flow rate $q \equiv Q/2VR$ versus gap-to-roll diameter ratio at same conditions as Figure 5. The different branches and turning points of the solution path are indicated

situation. The gap's influence at the chosen inflow boundary becomes appreciable close to turning point #2 and the flow rate Q becomes a function of the distance between the roll surfaces, H_0. Beyond this point, along segments C (unstable) and D (stable), q varies almost linearly with the gap, i.e. the actual flow rate Q is nearly proportional to the product of the gap and the roll speed. The proportionality factor λ ($\lambda \equiv Q/2\bar{V}H_0$) varies only from 1·33 to 1·37 over a wide range of gaps, indicating that the pressure in the inflow region does not change enough to affect much the flow through the gap. This is the *metering regime*, where the flow rate is controlled by the distance between the rolls. The *free boundary condition* admits this situation too.

As the gap is narrowed, all else being the same, the inflow region more closely resembles the half-flooded gap studied by Coyle *et al.*[2] The flow rate varies almost linearly with the clearance between the rolls. The results reported in Figure 7 show that the half-flooded hypothesis is adequate to describe metering gaps.

Turning points along the family of flow states mean that in at least some range of parameters there are two or more flow states at the same set of parameters. When three or more flow states occur, there is the possibility of hysteresis. For example, a pre-metered regime cannot be achieved starting from flow state (e) in Figure 5. As the gap is widened, the flow states evolve along branch D until a gap-to-diameter ratio $H_0/R \approx 0{\cdot}0125$ is reached. At any wider gap the coating bead breaks up.

The results in Figures 5 and 7 can be rearranged and plotted as dynamic contact line location versus dimensionless flow rate $\lambda \equiv Q/2H_0\bar{V}$, as illustrated in Figure 8. For the case of imposed inlet velocity profile (and therefore fixed flow rate), Benjamin[9] also plotted dynamic contact line position versus dimensionless flow rate λ and deduced the range of dimensionless flow rate in which two-dimensional, steady flows could exist at each capillary number. Turning point #1 clearly sets a minimum value of λ below which two-dimensional, steady states do not exist. However, there is no upper limit on λ, contrary to Benjamin's[9] finding. The dimensionless flow rate λ increases beyond the value at which the transition from a pre-metered to a metered regime occurs.

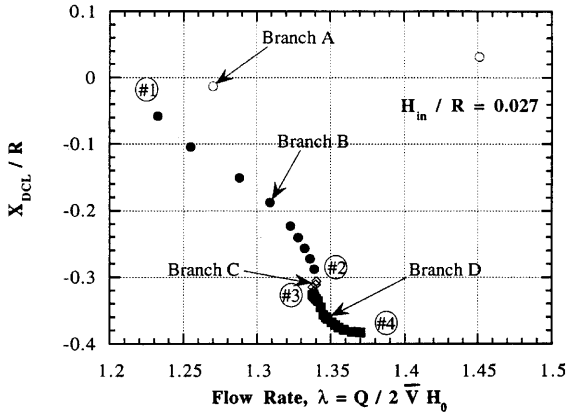

Figure 8. Solution path versus dimensionless flow rate $\lambda \equiv Q/2H_0\bar{V}$. Turning point #1 represents a minimum value of λ. There is no upper limit of λ, unlike the situation found by Benjamin[9] when the inlet velocity profile was fixed, even at a set of parameters at which the gap is operating in the metered regime

How the position of the dynamic contact line, X_{DCL}, and the flow rate $q \equiv Q/2\bar{V}R$ vary with the gap is shown in Figures 9 and 10; both figures are for an inlet film thickness of $H_{\mathrm{in}}/R = 0{\cdot}016$. The shape of the path of states is the same as in the case with $H_{\mathrm{in}}/R = 0{\cdot}027$ (Figures 5 and 7). Figure 11 combines Figures 7 and 10 into a plot of flow rate versus gap. As the rolls are brought closer together, the flow rate gradually becomes affected by the distance between the rolls and gradually the premetered regime turns into the metered regime. In the metered regime the relation between flow rate and gap is independent of the incoming film thickness H_{in}, as expected, and follows the almost linear relation between the flow rate Q and gap H_0 that exists in the fully flooded flow states reported by Coyle *et al.*[2] The range of gaps at which stable pre-metered flows exist varies with the inlet thickness.

Figure 12 compiles all the results in this section into an operability window in the plane of gap–inlet layer thickness. The pre-metered regime region is bounded by the limit points of coating bead

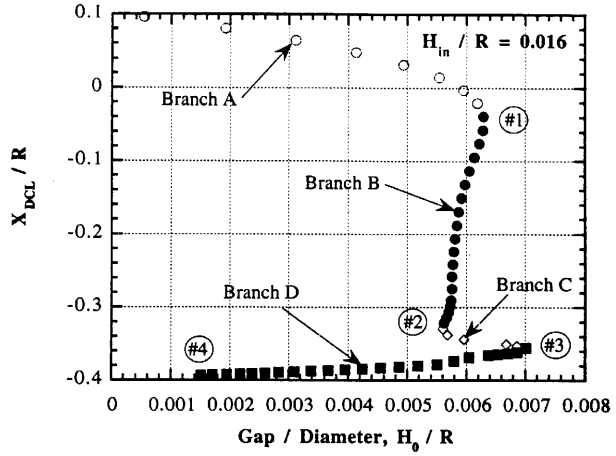

Figure 9. Path of flow states at $St = 0, Ca = 0{\cdot}1, Re \times R/H_0 = 100$ and $H_{\mathrm{in}}/R = 0{\cdot}016$. The states are characterized by the position of the dynamic contact line, X_{DCL}, which is where the liquid meets the metering roll

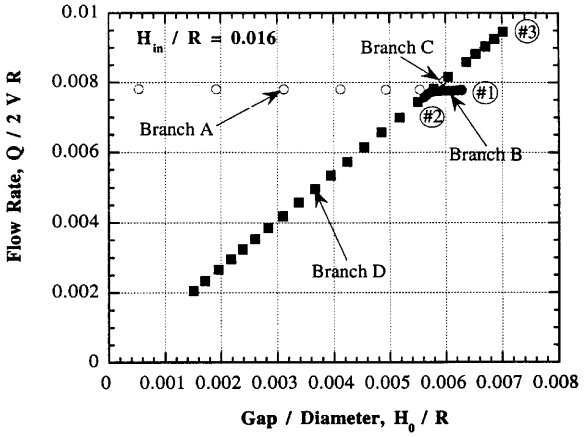

Figure 10. Flow rate $q \equiv Q/2\bar{V}R$ versus gap-to-diameter ratio. $H_{in}/R = 0{\cdot}016$. Along most of branch B the flow rate is virtually constant (pre-metered regime); then it gradually becomes a linear function of the distance between the rolls

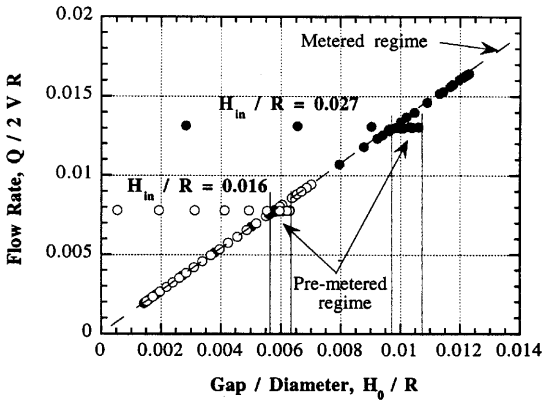

Figure 11. Comparison between the flow rate $q \equiv Q/2\bar{V}R$ versus gap at $H_{in}/R = 0{\cdot}027$ and $0{\cdot}016$. The range of gaps at which the flow rate is virtually constant, i.e. the pre-metered regime, is highlighted at each inlet thickness

existence and by the metered regime region. At a given gap-to-diameter ratio, if the inlet layer thickness is too small, no coating bead can be formed and sustained. If it is somewhat larger but still smaller than the distance between the rolls, the coating bead cannot be formed without assistance, but once formed it can be sustained. The flow is in the pre-metered regime. If the incoming film is still thicker, recirculations appear on the inlet side of the gap and the flow rate gradually becomes controlled by the flow between the rolls, i.e. a metering regime is established.

3.2. Single-film-fed forward-roll coating in the presence of gravity

Whereas gravity was set to zero ($St = 0$) in the preceding subsection, it is not in this subsection. Although gravity affects negligibly the region of lubrication flow between the rolls, it can appreciably affect the flow beneath the free surface on the inflow side of the gap. The flow states in this section were obtained at $St^* \equiv St \times (R/H_0)^2 = 1{\cdot}4 \times 10^4 (\rho \approx 10^3 \text{ kg m}^3, \quad g \approx 10 \text{ m s}^{-1}, R \approx 10 \text{ cm}, \mu \approx 10 \text{ cP}$ and $V \approx 1 \text{ m s}^{-1}$.

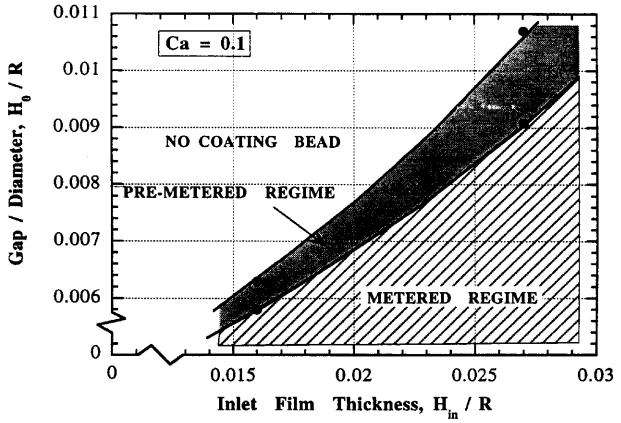

Figure 12. Operability window of forward-roll coating in absence of gravity in plane of inlet thickness H_{in} versus gap H_0. $Ca = 0{\cdot}1$, $St = 0$ and $Re \times R/H_0 = 100$

The structure of the solution paths is similar to that of the paths plotted in the preceding section, as shown in Figure 13. This figure illustrates the variation in dynamic contact line position with the distance between the rolls. The path of flow states was computed at $Ca = 0{\cdot}1$, $St^* = 1{\cdot}4 \times 10^4$, $Re \times R/H_0 = 100$ and $H_{in}/R = 6{\cdot}1 \times 10^{-3}$. The topmost branch in Figure 13 (branch A) is likely to be unstable and in extreme cases, i.e. smaller gaps, would probably lead to defective films, because the dynamic contact line is located downstream of the plane of minimum gap. Turning point #1, between branches A and B, sets an upper limit on the gap: two-dimensional steady states do not exist above this limit, i.e. the coating bead breaks up when the rolls are moved farther apart. The position of the dynamic contact line is a very strong function of the gap along most of branch B and moves upstream as the clearance between the rolls diminishes until very close to turning point #2 (see flow states (a) and (b) in Figure 15). Beyond this flow state, along the remainder of branch B and along branches C and D, the dynamic contact line position is almost insensitive to the gap setting. Although this feature is hard to discern, the final portion of branch B and branches C and D are folded.

There is no recirculating gyre on the inflow side of the gap along most of branch B. The gyre appears just before turning point #2 on the path of states. After that, along branch D, which corresponds to the other set of stable states, the recirculation zone extends upstream, i.e. expands down the incoming layer as the rolls are brought together and the gap reduced, as depicted in flow states (c) and (d) of Figure 14. Turning point #4 occurs when the recirculation zone reaches the synthetic inflow boundary. At this stage the inlet layer thickness can no longer be imposed. The condition at the corner between the inflow plane and the upstream free surface is switched from setting the inlet film thickness to the weighed kinematic condition, as explained in Section 2. The flow states of this second sequence of predictions are also shown in Figure 13—flow states (e)–(g). As the gap is narrowed, the plane at which the velocity first reverses at the free surface moves upstream, as illustrated in Figure 15, and finally crosses the synthetic inflow boundary: flow state (g). The free boundary condition allows this transition from a no-run-back velocity profile to a run-back velocity profile in the arriving layer. The streamlines of representative flow states that are labelled in Figure 13 are shown in Figure 14.

Figure 16 shows how the dimensionless flow rate $q \equiv Q/2\bar{V}R$ varies with the gap. It does not vary perceptibly along most of branch B: the flow is virtually pre-metered and the flow rate is set by the arriving layer or film of liquid. Close to turning point #2 the flow rate Q gradually changes until it

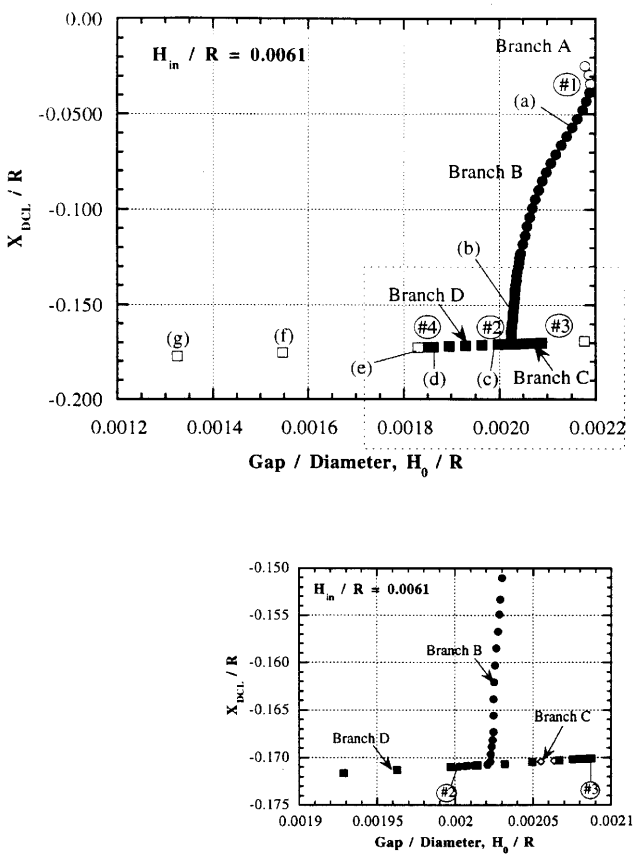

Figure 13. Path of flow states (solutions of governing equations) at $St^* \equiv St \times (R/H_0)^2 = 1{\cdot}4 \times 10^4$, $Ca = 0{\cdot}1$, $Re \times R/H_0 = 100$ and $H_{in}/R = 6{\cdot}1 \times 10^{-3}$. The states are characterized by the position of the dynamic contact line, X_{DCL}, which is where the liquid meets the metering roll

varies with the gap in an almost linear manner. Along the entire solution branch D the flow rate Q is a nearly linear function of the distance between the rolls, in the same way as when the upstream side of the gap is totally flooded, i.e. the 'half-flooded' regime studied by Coyle *et al.*[9] In these conditions the flow is metered by the gap and the flow rate is not known *a priori*. The solutions of the equation system that includes the weighted kinematic residual in place of the equation that fixes the inlet layer thickness are also shown. They prove to be virtually indistinguishable from a continuation of branch D. When the inflow film thickness is set at $H_{in}/R = 6{\cdot}1 \times 10^{-3}$, the range of dimensionless gaps that admit the pre-metered regime is from $2{\cdot}02 \times 10^{-3}$ to $2{\cdot}2 \times 10^{-3}$. The flow gradually becomes metered below the lower limit and the coating bead breaks up above the upper limit.

Figure 17 shows the flow state path at $Ca = 0{\cdot}5$. The structure is the same as the flow state path at $Ca = 0{\cdot}1$ in Figure 13. Again the pre-metered regime extends over a range of gap-to-roll diameter ratios. Above the upper limit the coating bead cannot exist and below the lower bound the inlet side becomes flooded and the flow rate is controlled by the flow between the rolls, the characteristics of a metering regime.

By tracking the range of gaps that bounds the pre-metered regime at different capillary numbers, an operating window can be constructed. An operating window at $H_{in}/R = 6{\cdot}1 \times 10^{-3}$ is shown in Figure 18. Above the upper curve, i.e. at large roll-to-gap ratios, no coating bead is possible. There is

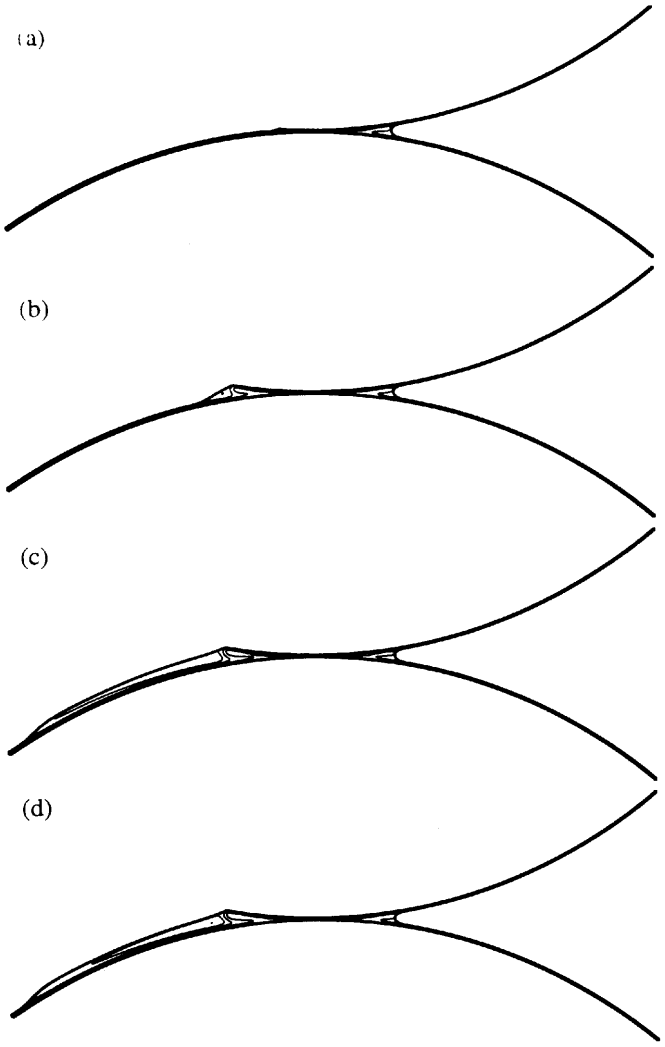

Figure 14. Streamlines of solutions labelled in Figure 13. The inlet thickness is fixed at $H_{in}/R = 6{\cdot}1 \times 10^{-3}$

a narrow range of gaps in which the flow is pre-metered and at small gaps the flow is in the metering regime. The pre-metering range broadens as the capillary number falls, i.e. as the roll speed decreases. At low capillary numbers, i.e. when capillary forces are much stronger than viscous forces, a coating bean can still exist, even when the distance between the rolls is large; it is then supported by the action of surface tension.

4. FINAL REMARKS

The transition from the pre-metered flow regime to the metering flow regime in single-film-fed forward-roll coating flow takes place as the gap is narrowed when the thickness of the incoming film is held constant. It also takes place when the gap is held fixed and the arriving thickness is raised. Similarly, the reverse transition, from metering to pre-metered flow, takes place as either the gap is

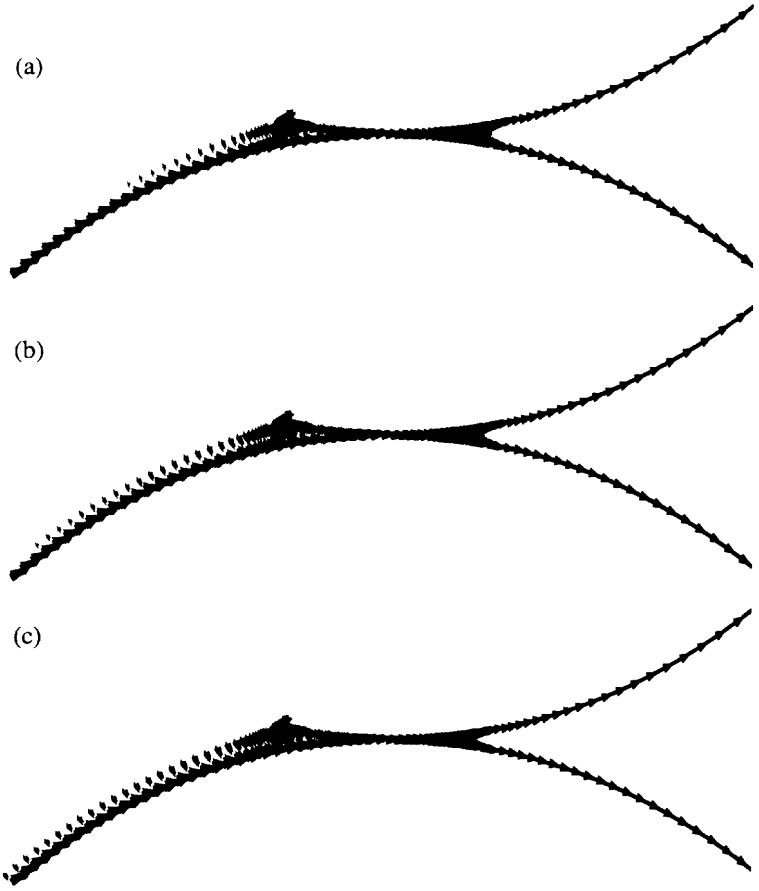

Figure 15. Velocity vectors in flow states marked (e)–(g), marked in Figure 13. The inlet layer thickness is not fixed

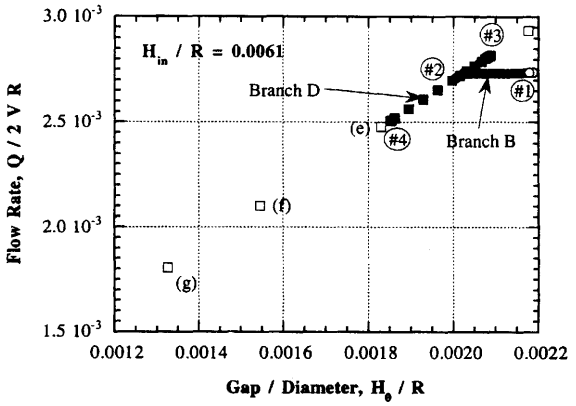

Figure 16. Dimensionless flow rate $q \equiv Q/2\bar{V}R$ versus gap-to-diameter ratio at $St^* \equiv St \times (R/H_0)^2 = 1{\cdot}4 \times 10^4$, $Ca = 0{\cdot}1$, $Re \times R/H_0 = 100$ and $H_{in}/R = 6{\cdot}1 \times 10^{-3}$. Flow states (e)–(g) are obtained when the equation that fixes the inlet thickness is replaced by the equation of vanishing weighted residual of the kinematic boundary condition adjacent to the synthetic inflow boundary

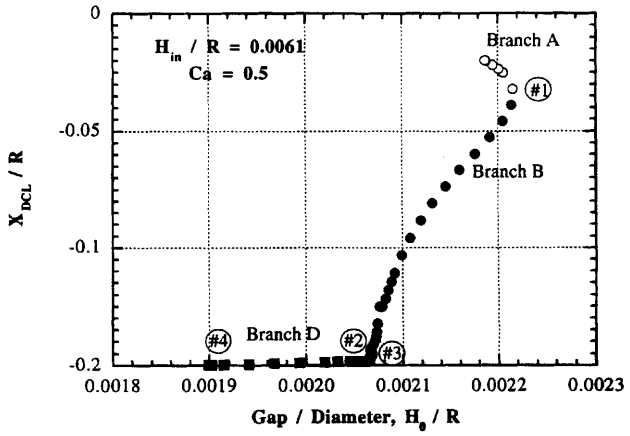

Figure 17. Path of states at $Ca = 0{\cdot}5$, $St^* \equiv St \times (R/H_0)^2 = 1{\cdot}4 \times 10^4$, $Re \times R/H_0 = 100$ and $H_{in}/R = 6{\cdot}1 \times 10^{-3}$. The states are characterized by the dynamic contact line position as in preceding figures

widened or the arriving thickness is lowered. However, there is hysteresis in these transitions, because the complete sequence of flow states as the gap is varied has turning points—as many as three turning points.

The full sequence of flow states has here been closely approximated by employing the *free boundary condition* advocated by Papanastasiou *et al.*[10] at the synthetic inflow boundary, together with a careful switch between (i) specifying the thickness of the inflowing layer of liquid and (ii) specifying a weighted residual of the kinematic boundary condition on the free surface segment adjacent to the inflow boundary. Alternative (i) accommodated the transition from the pre-metered regime to the metering regime. However, as the gap was narrowed and the recirculating flow (rolling bank) came close to the inflow plane, the solutions of the equation system developed unrealistic free surface shapes, evidently in order to accommodate both the requirement of mass conservation and the imposed film thickness. Then the switch was made to alternative (ii), which at the same gap gave *very* nearly the *same* flow rate and location of the dynamic contact line (see Figures 13 and 16). At

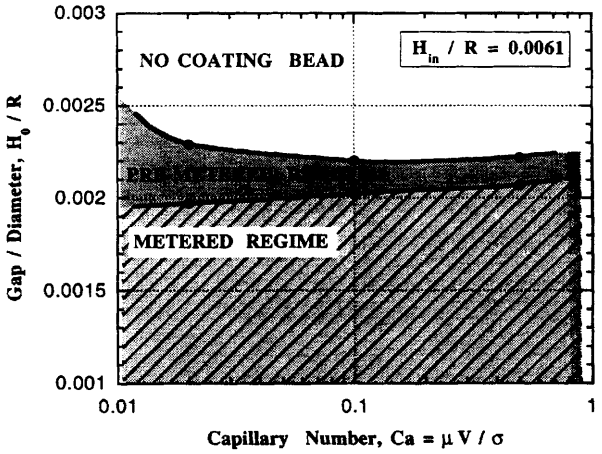

Figure 18. Flow regime map of single-film-fed forward-roll coating flows in plane of gap-to-diameter ratio and capillary numbers. $St^* \equiv St \times (R/H_0)^2 = 1{\cdot}4 \times 10^4$, $Re \times R/H_0 = 100$ and $H_{in}/R = 6{\cdot}1 \times 10^{-3}$

narrower gaps the second alternative accommodates flow states in which liquid runs back from the gap over the liquid dragged towards the gap by the roll surface. When the two sequences of flow states are plotted as in Figures 13 and 16, they lie close enough together that they appear to define a continuous curve.

In summary, the predictions computed from the theory reveal an upper limit on the gap-to-roll diameter ratio above which the coating bead breaks up; they show the existence of multiple (up to four) steady states, which raises the possibility of hysteresis; and they illustrate the transition from pre-metered to metering flows.

Figures 12 and 18 are examples of flow regime maps that portray the parameter range in which the coating bead can exist and the ranges in which a coating gap operates in either a pre-metered or a metering regime.

ACKNOWLEDGEMENTS

M. S. Carvalho was supported by a fellowship from CAPES (Brazilian Federal Government). Further support came from co-operating corporations through the Center for Interfacial Engineering and was supplemented by the National Science Foundation and the Minnesota Supercomputer Institute.

REFERENCES

1. M. D. Savage, P. H. Gaskell and J. L. Summers, 'Flow transformation from classical to meniscus forward roll coating', *AIChE Spring Natl. Meet.*, Atlanta, GA, 1994.
2. D. J. Coyle, L. E. Scriven and C. W. Macosko, (1986) 'Film splitting flows in forward roll coating', *J. Fluid Mech.*, **171**, 183 (1986).
3. E. Pitts and J. Greiller, 'The flow of thin liquid films between rollers', *J. Fluid Mech.*, **11**, 33 (1961).
4. J. Greener and S. Middleman, 'A theory of roll coating of viscous and viscoelastic fluids', *Polym. Eng. Sci.*, **15**, 1 (1975).
5. K. S. A. Chen and B. G. Higgins, 'Study of the flow in the upstream bank of liquid in a forward roll coater by the finite element method', *Chem. Eng. Sci.*, **43**, 2867 (1988).
6. K. S. A. Chen and L. E. Scriven, 'Roll coating, forward and reverse: effect of feed condition', *AIChE Spring Nat. Meet.*, New Orleans, LA, 1988.
7. J. L. Bourgeois and J. F. Agassant, 'Calendering of PVC', *J. Macromolec. Sci.-Phys.*, **B14**, 367 (1977).
8. J. F. Agassant and M. Epsy, 'Theoretical and experimental study of the molten polymer flow in the calendar bank', *Poly. Eng. Sci.*, **25**, 118 (1985).
9. D. F. Benjamin, 'Roll coating flows and multiple flow systems', *Ph.D. Thesis*, University of Minnesota, Minneapolis, MN, University Microfilms International, Ann Arbor, MI. 1994.
10. T. C. Papanastasiou, N. Malamataris and K. Ellwood, 'A new outflow boundary condition', *Int. j. numer. methods fluids*, **14**, 587 (1992).
11. R. L. Sani and P. M. Gresho, 'Résumé and remarks on the open boundary condition minisymposium', *Int. j. numer. methods fluids*, **18**, 983 (1994).
12. S. F. Kistler and L. E. Scriven, 'Coating flows', in J. R. A. Pearson and S. M. Richardson (eds), *Computational Analysis of Polymer Processing*, Applied Science Publishers, London, 1983, p. 243.
13. J. F. Thompson *et al.*, *Numerical Grid Generation*, Elsevier Science Publ., New York, 1985.
14. J. E. Castillo, *Mathematical Aspects of Numerical Grid Generation*, SIAM, Philadelphia, 1991.
15. P. M. Knopp and S. Steinberg, *The Fundamentals of Grid Generation*, CRC Press, Boca Raton, FL, 1993.
16. J. M. de Santos, 'Two-phase cocurrent downflow through constricted passages', *Ph.D. Thesis*, University of Minnesota, Minneapolis, MN, University Microfilms International, Ann Arbor, MI. 1990.
17. K. N. Christonoulou, 'Computational physics of slide coating flow', *Ph. D. Thesis*, University of Minnesota, Minneapolis, MN, University Microfilms International, Ann Arbor, MI, 1990.
18. H. B. Keller, 'Numerical solution of bifurcation and nonlinear eigenvalue problems', in P. H. Rabinowitz (ed.), *Applications of Bifurcation Theory*, 1977.
19. G. Iooss and D. D. Joseph, *Elementary Stability and Bifurcation Theory*, Springer, New York, 1980.
20. K. Adachi, T. Tamura and R. Nakamura, 'Coating flows in a nip region and various critical phenomena', *AIChE J.*, **34**, 456 (1988).
21. M. S. Carvalho, 'Roll coating flows in rigid and deformable gaps', *Ph.D. Thesis*, University of Minnesota, Minneapolis, MN, University Microfilms International, Ann Arbor, MI, 1990.

22. J. Greener, T. Sullivan, B. Turner and S. Middleman, 'Ribbing instability of a two-roll coater: Newtonian fluids', *Chem. Eng. Commun.*, **5**, 73 (1980).
23. P. M. Gresho and R. L. Lee, 'Don't suppress the wiggles—they're telling you something', *Comput. Fluids*, **9**, 223 (1981).
24. P. M. Gresho and R. L. Sant, 'On pressure boundary conditions for the incompressible Navier–Stokes equations', *Int. j. numer. methods fluids*, **7**, 1111 (1987).
25. P. M. Gresho, 'Some current CFD issues relevant to the incompressible Navier–Stokes equations', *Comput. Methods Appl. Mech. Eng.*, **87**, 201 (1991).
26. P. M. Gresho, 'Some interesting issues in incompressible fluid dynamics, both in the continuum and in numerical simulation', in T. E. Tezduyar (ed.), *Advances in Applied Mechanics*, Academic, New York, 1992.

